Letter

Mechanism of Molecular Polariton Decoherence in the Collective Light−Matter Couplings Regime

Benjamin X. K. Chng, Wenxiang Ying, Yifan Lai, A. Nickolas Vamivakas, Steven T. Cundiff, Todd D. Krauss, and Pengfei Huo*

Read Online

| ACCESS | | Metrics & More | | Article Recommendations | | Supporting Information |

ABSTRACT: Molecular polaritons, the hybridization of electronic states in molecules with photonic excitation inside a cavity, play an important role in fundamental quantum science and technology. Understanding the decoherence mechanism of molecular polaritons is among the most significant fundamental questions. We theoretically demonstrate that hybridizing many molecular excitons in a cavity protects the overall quantum coherence from phonon-induced decoherence. The polariton coherence time can be prolonged up to 100 fs with a realistic collective Rabi splitting and quality factor at room temperature, compared to the typical electronic coherence time which is around 15 fs. Our numerically exact simulations and analytic theory suggest that the dominant decoherence mechanism is the population transfer from the upper

polariton state to the dark state manifold. Increasing the collective coupling strength will increase the energy gap between these two sets of states and thus prolong the coherence lifetime. We further derived valuable scaling relations that directly indicate how polariton coherence depends on the number of molecules, Rabi splittings, and light−matter detunings.
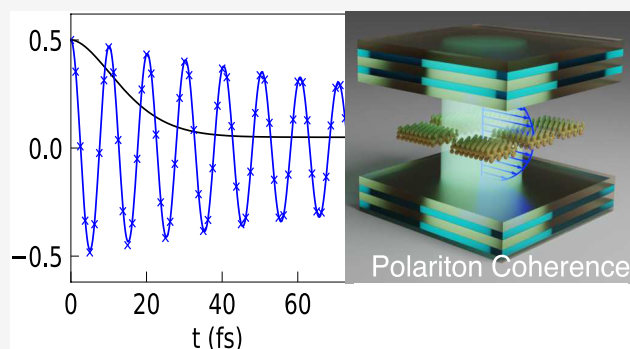
N ovel quantum systems are an emerging technology that promises significant advancement and understanding in the fields of quantum computing, quantum information science, and fundamental quantum optics research. A quantum system of significant interest is the optical cavity polariton,[1−3] which are formed from interactions between electronic states in matter systems and the quantized radiation field in a cavity. Properties of such optical cavity polaritons have been exploited to realize phenomena such as polariton lasing,[4−7] Bose−Einstein condensation,[8−12] making integrated circuit elements that can be optically switched,[13−15] and achieving long-range polariton transport.[16−19] In particular, forming polaritons with molecules or nanoparticles has garnered much attention recently, and the resulting hybridized states are known as molecular polaritons.[20−23] Like polaritons formed from an atom's electronic states, these molecular polaritons exhibit properties that are derived from both the matter excitations and the photonic components inside a cavity. However, these molecular polaritons possess additional vibrational states from their matter excitations that affect transduction between the matter and photonic degrees of freedom (DOF). These additional states offer new opportunities in the fields of quantum chemistry and quantum materials, as the physical properties of the constituent molecules can be tuned via strong light−matter interactions. For instance, the potential energy surfaces of molecules coupled to a cavity photon can be modified by changing its light−matter coupling strength or the

frequency of the cavity mode,[24−26] hence, providing new pathways for chemical reactions to occur.

To exploit the desired properties of molecular polaritons, we need to preserve the hybridized state for the duration of the relevant quantum process. The key measure is therefore the degree of quantum coherence, which characterizes how long the quantum states involved can interfere with each other.[27] It has been shown that interactions of the molecules with the environment, such as cavity loss or phonon-induced decoherence,[28,29] occur rapidly on a time scale of several femtoseconds and this constrains the ability of the molecular polariton to last throughout the desired quantum processes.[30] However, previous work has shown that coupling a single molecule to a cavity significantly enhances the coherence lifetime of the hybrid light−matter system.[31,32] Furthermore, recent work has established that coupling many molecules into a cavity reduces the effective reorganization energy of the polariton states.[33−35] This collective coupling effect reduces the coupling strength between the molecular electronic states

and their respective phonon modes,[36] and thus impacts their coherence lifetimes.

In this Letter, we address the effect of coupling many molecules into a cavity on the coherence lifetimes of the polaritonic states. The coherences of a model light−matter Hamiltonian with many molecules were examined and exact quantum dynamics, based on the hierarchical equation of motion (HEOM) formalism,[37−39] is performed on this model Hamiltonian. We demonstrate through numerical results from HEOM that the coherence lifetimes increase with the collective light−matter coupling strength. Moreover, we explain the enhancement in the polariton's coherence lifetime using Fermi's golden rule (FGR) argument in the frequency domain, and this accounts for the scaling of the coherence lifetimes with respect to the number of molecules and the single molecule light−matter coupling strength.

To model the collective light−matter coupling between N molecules and a quantized cavity mode, we use the Holstein-Tavis-Cummings (HTC) Hamiltonian[40−43]

$$\hat{H}_{HTC} = \hat{H}_M + \hat{H}_{ph} + \hat{H}_{LM} \tag{1}$$

where $\hat{H}_M$ is the matter Hamiltonian that describes N identical and noninteracting molecules, $\hat{H}_{ph}$ describes the photon field Hamiltonian, and $\hat{H}_{LM}$ describes the light−matter interactions.

For the matter Hamiltonian, we consider N identical molecules, each containing two electronic states $\{|g\rangle, |e\rangle\}$, where $|g\rangle$ and $|e\rangle$ are the ground and excited states of the molecule, respectively. We further denote the exciton raising and lowering operators

$$\hat{\sigma}_n^\dagger = |e_n\rangle\langle g_n|; \qquad \hat{\sigma}_n = |g_n\rangle\langle e_n| \tag{2}$$

which create and annihilate an exciton on the n_{th} molecule. The matter Hamiltonian is expressed as

$$\hat{H}_M = \sum_{n=0}^{N-1} \left[(\omega_x + \lambda)\hat{\sigma}_n^\dagger\hat{\sigma}_n + \sum_\alpha \omega_\alpha \left(\hat{b}_{\alpha,n}^\dagger \hat{b}_{\alpha,n} + \frac{1}{2} \right) \right.$$
$$\left. + \hat{\sigma}_n^\dagger\hat{\sigma}_n \sum_\alpha c_\alpha(\hat{b}_{\alpha,n}^\dagger + \hat{b}_{\alpha,n}) \right] \tag{3}$$

Further, λ is the reorganization energy, due to the exciton−phonon coupling, where the *diabatic* excitation energy between the two states is $\hbar\omega_x = E_e - E_g$ (and throughout the work, we will set $\hbar = 1$) for all $n \in [0, N-1]$ molecules. Each molecule contains a set of phonon vibrations. The phonon DOFs of the molecules are considered as the bath Hamiltonian, which couple to the system through the system-bath (exciton−phonon) coupling, expressed as follows (c.f. eq 2)

$$\hat{H}_b = \sum_{n=0}^{N-1} \sum_\alpha \omega_\alpha \left(\hat{b}_{\alpha,n}^\dagger \hat{b}_{\alpha,n} + \frac{1}{2} \right) \tag{4a}$$

$$\hat{H}_{sb} = \sum_{n=0}^{N-1} \hat{\sigma}_n^\dagger\hat{\sigma}_n \sum_\alpha c_\alpha(\hat{b}_{\alpha,n}^\dagger + \hat{b}_{\alpha,n}) \tag{4b}$$

where ω_α are the frequencies for the α_{th} phonon mode, $\hat{b}_{\alpha,n}^\dagger$ and $\hat{b}_{\alpha,n}$ are the bath phonon creation and annihilation operators that satisfy the bosonic commutation relations. $\hat{H}_{sb}$ describes the system-bath interaction, where c_α denotes the coupling

strength between the molecules and the α-th bath phonon mode. The system-bath interactions are determined by the spectral density[44,45]

$$J_\nu(\omega) = \pi \sum_\alpha c_\alpha^2 \delta(\omega - \omega_\alpha) = \frac{2\lambda\gamma\omega}{\gamma^2 + \omega^2} \tag{5}$$

where we use the Drude-Lorentz model, γ is the bath characteristic frequency, and the reorganization energy (inside $\hat{H}_M$) is $\lambda = \sum_\alpha c_\alpha^2/\omega_\alpha = (1/\pi)\int_0^{+\infty} d\omega J(\omega)/\omega$ for all molecules. Here, we use the following parameters: excitation energy $\omega_x = 2.0$ eV, the bath reorganization energy $\lambda = 30$ meV, and the bath characteristic frequency $\gamma = 24.8$ meV, which are the typical parameters for CdSe Nanoplatelets (see schematic illustration in Figure 1a) which has been shown to couple strongly to a dielectric optical cavity.[42,46]

Further, $\hat{H}_c$ describes a single quantized radiation mode inside the cavity

$$\hat{H}_c = \omega_c \left(\hat{a}^\dagger\hat{a} + \frac{1}{2} \right) \tag{6}$$

where ω_c is the photon frequency of the cavity mode, and $\hat{a}^\dagger$ and $\hat{a}$ are the creation and annihilation operators for a photon in the cavity mode. For the light−matter interaction term $\hat{H}_{LM}$, we assume that each molecule is coupled to the quantized radiation field with the same light−matter coupling strength g_c. Under the rotating wave approximation, $\hat{H}_{LM}$ is expressed as

$$\hat{H}_{LM} = g_c \sum_{n=0}^{N-1} (\hat{a}^\dagger\hat{\sigma}_n + \hat{a}\hat{\sigma}_n^\dagger) \tag{7}$$

Note that when entering into the ultrastrong coupling regime $\sqrt{N}g_c/\omega_c > 0.1$, one needs to incorporate the counter-rotating wave terms $(\hat{a}^\dagger\hat{\sigma}_n^\dagger$ and $\hat{a}\hat{\sigma}_n)$ and dipole-self-energies to accurately describe the light−matter interaction.[43,47] We restrict our parameters away from the ultrastrong coupling regime.[47]

In this work, we consider the single excitation subspace

$$|G, 1\rangle = |g_0\rangle \otimes ...|g_n\rangle... \otimes |g_{N-1}\rangle \otimes |1\rangle \tag{8a}$$

$$|E_n, 0\rangle = |g_0\rangle \otimes ...|e_n\rangle... \otimes |g_{N-1}\rangle \otimes |0\rangle \tag{8b}$$

where $|G, 1\rangle$ represent the 1-photon-dressed ground state, and $|E_n, 0\rangle$ represent the single excited state for the n_{th} molecule. In the above single excitation manifold, the collective "bright" excitonic state is

$$|B\rangle = \frac{1}{\sqrt{N}} \sum_{n=0}^{N-1} |E_n, 0\rangle \tag{9}$$

which couples to the $|G, 1\rangle$ state through the light−matter interaction term $\hat{H}_{LM}$, resulting in the light−matter hybridized states that are known as polaritons.

We further define the following diabatic Polariton Hamiltonian, which refers to the "system" Hamiltonian

$$\hat{H}_s = \sum_{n=0}^{N-1} (\omega_x + \lambda)\hat{\sigma}_n^\dagger\hat{\sigma}_n + \hat{H}_{ph} + \hat{H}_{LM} \tag{10}$$

which contains the excitonic DOF, the cavity mode, and the light−matter coupling terms. There are a total of $N + 1$
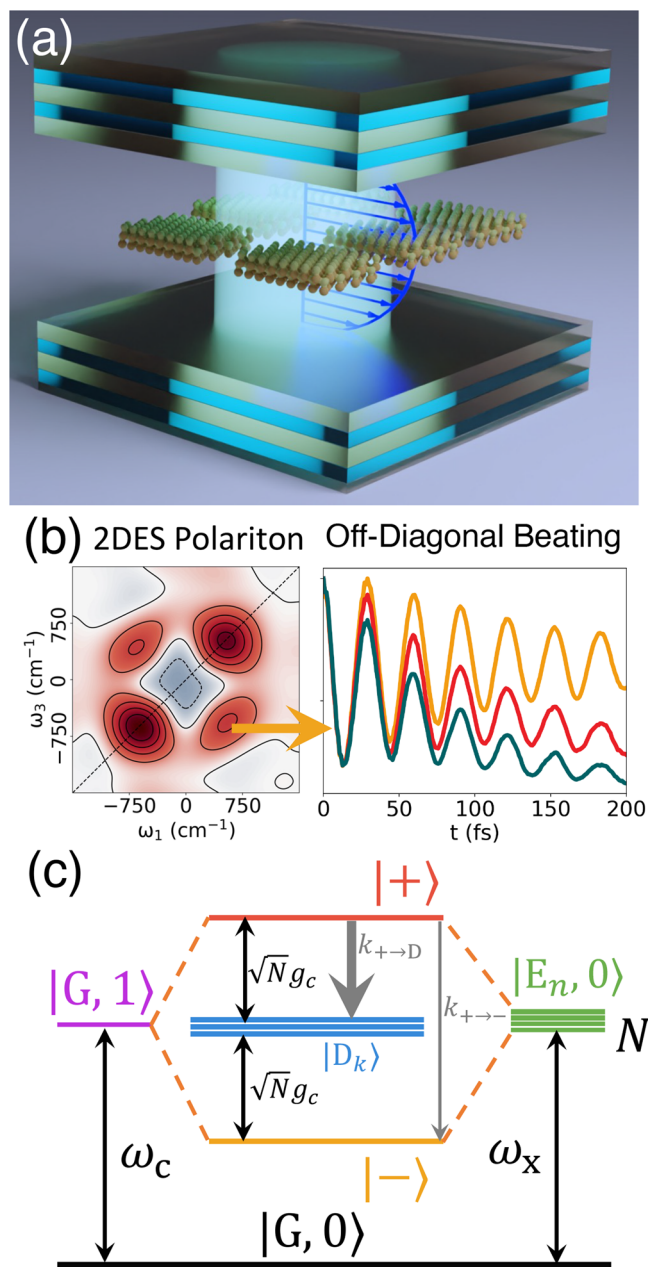
Figure 1. (a) Schematic illustrations of many emitters coupled to the quantized radiation field inside an optical cavity. (b) Schematic illustrations of 2DES spectroscopy with the off-diagonal beating signal corresponding to the polaritonic coherence $\rho_{+-}(t)$. (c) The energy level of the HTC model depicts the hybridization of matter and photonic states to form polariton states.

eigenstate of $\hat{H}_S$ in the first excitation subspace (because there are $N + 1$ basis states, see eq 8), among which there are two bright polariton states,[48] commonly referred to as the Upper polariton (UP) state $|+\rangle$ and the Lower polariton (LP) state $|-\rangle$, expressed as

$$|+\rangle = \cos\Theta_N |B\rangle + \sin\Theta_N |G, 1\rangle \tag{11a}$$

$$|-\rangle = -\sin\Theta_N |B\rangle + \cos\Theta_N |G, 1\rangle \tag{11b}$$

where Θ_N is the mixing angle between light and matter

$$\Theta_N = \frac{1}{2}\tan^{-1}\left(\frac{2\sqrt{N}g_c}{-\Delta}\right) \tag{12}$$

where the angle is defined in the range of $\Theta_N \in [0, \pi/2]$, and the light−matter detuning is defined as[48]

$$\Delta = \omega_c - (\omega_x + \lambda) \tag{13}$$

When $\Delta = 0$, the mixing angle becomes $\Theta_N = \pi/4$, the polariton states become

$$|\pm\rangle = \frac{1}{\sqrt{2}}[|G, 1\rangle \pm |B\rangle] \tag{14}$$

and the Rabi splitting (energy gap) between the $|+\rangle$ and $|-\rangle$ is

$$\Omega_R = 2\sqrt{N}g_c \tag{15}$$

The remaining $N - 1$ eigenstates are referred to as the "Dark states", expressed as

$$|D_k\rangle = \frac{1}{\sqrt{N}}\sum_{n=0}^{N-1}\exp\left(-2\pi i\frac{nk}{N}\right)|E_n, 0\rangle \tag{16}$$

where the coefficients $\sum_{n=0}^{N-1}\exp\left(-2\pi i\frac{nk}{N}\right) = 0$. These Dark states also satisfy $\langle G, 0|\hat{\mu}|D_k\rangle = 0$ due to the zero-sum property of the expansion coefficients, and as such, direct optical transition is not allowed and they are thus dark in spectra. Note that the $|\pm\rangle$ polariton states and the dark states manifold $\{|D_k\rangle\}$ are "diabatic" states in their nature because they are the eigenstates of $\hat{H}_s$ (eq 10), and their character do not change as a function of nuclear configuration $\hat{R}_{\alpha,n} = (\hat{b}_{\alpha,n}^{\dagger} + \hat{b}_{\alpha,n})/\sqrt{2}$. On the other hand, one can also define polariton states as the eigenvector of the adiabatic polariton Hamiltonian[42,46] $\hat{H}_{pl} = \hat{H} - \hat{T}_R$, where $\hat{T}_R$ is the nuclear kinetic energy operator (for all phonons). The eigenstates of $\hat{H}_{pl}$ can be viewed as the adiabatic version of the polariton and dark states because the state character explicitly depends on nuclear configuration $\{\hat{R}_{\alpha,n}\}$, and it has been used to interpret the photoluminescence spectra[42,46,49,50] or investigate coherences in polariton transport.[18,51,52]

Our focus is the coherence between $|+\rangle$ and $|-\rangle$ states, which is directly related to the off-diagonal beating in 2DES spectra and has been experimentally explored (see Figure 1b).[36] To probe the polariton coherences, we compute the off-diagonal matrix elements of the system-reduced density matrix (RDM), defined as

$$\rho_{+-}(t) = \langle+|\hat{\rho}_s(t)|-\rangle = \langle+|Tr_b[\hat{\rho}(t)]|-\rangle \tag{17}$$

where $\hat{\rho}$ denotes the full density operator and $\hat{\rho}_s$ is the RDM operator for the system by tracing out the bath DOF. Note that the coherence in this definition is basis-dependent and can lead to qualitatively different results with a change of basis when analyzing decoherence dynamics. Purity, $Tr_s[\hat{\rho}_s^2(t)]$ on the other hand, is representation-independent. Here, we investigate $\rho_{+-}(t)$ because it is closely connected with the 2DES spectra measured experimentally (off-diagonal beating signals which correspond to the cross peak of $|+\rangle$ and $|-\rangle$ states). We also present the results of purity in Sec. IV of the Supporting Information. The population and coherence are obtained by performing exact quantum dynamics simulation using the

HEOM method.[37−39] The system Hamiltonian $\hat{H}_s$ is represented in the single excitation subspace (eq 8), and the bath and system-bath part $\hat{H}_b + \hat{H}_{sb}$ are described by the spectral density (eq 5). The details of the simulations are provided in Sec. III of the Supporting Information.

For all simulations (except in Figure 7), we consider a resonant condition of light−matter interaction $\Delta = 0$ (see expression in eq 13). The initial condition is assumed to be separable as

$$\hat{\rho}(0) = \hat{\rho}_s(0) \otimes \hat{\rho}_b(0) = |\Psi(0)\rangle\langle\Psi(0)| \otimes \frac{1}{\mathcal{Z}_b}e^{-\beta\hat{H}_b} \tag{18}$$

where the system is initially prepared in a pure state

$$|\Psi(0)\rangle = |B\rangle = \frac{1}{\sqrt{2}}(|+\rangle - |-\rangle) \tag{19}$$

The bath is assumed to be in thermal equilibrium, where $\mathcal{Z}_b = \mathrm{Tr}[e^{-\beta\hat{H}_b}]$ is the partition function, with $\beta = 1/k_BT$ and we consider $T = 300$ K throughout this work. To compare the decoherence dynamics outside the cavity, we take the $g_c = 0^+$ limit, such that the mixing angle $\lim_{g_c \to 0^+} \Theta_N = \pi/4$ under the resonant condition (see eq 12). Thus, the initial condition $|\Psi(0)\rangle$ for the outside cavity case can still be interpreted in eq 19, and under the $g_c = 0^+$ limit one still have well-defined states $|\pm\rangle = \frac{1}{\sqrt{2}}[|G, 1\rangle \pm |B\rangle]$ to probe their coherence. The meaning of the $g_c \to 0^+$ limit is actually the decoherence among $|E_n, 0\rangle$ in the $|B\rangle = \frac{1}{\sqrt{N}}|E_n, 0\rangle$ state, due to the coupling of $|E_n, 0\rangle$ with its own individual bath. We return to detailed discussions of the above in Sec. VII of the Supporting Information.

Figure 2 presents $\mathrm{Re}[\rho_{+-}(t)]$, the real part of the coherence between the $|+\rangle$ and $|-\rangle$ states, in a lossless cavity (no photon decay). Here, we fix the number of molecules $N = 10$, and the collective coupling strength $\sqrt{N}g_c$ varies from 100 to 200 meV by changing g_c. The black solid line corresponds to the coherence under the limit of $g_c = 0^+$ (outside the cavity), where $\rho_{+-}(t)$ decays with a Gaussian profile which is consistent with the established result of Gaussian coherence decay.[53] Panel (a)-(c) preset the decoherence process with $\rho_{+-}(t)$ by gradually increasing the light−matter coupling strength g_c. One can see that an increase in $\sqrt{N}g_c$ can significantly prolong the coherence time. An interesting feature we observed is that $\rho_{+-}(t)$ switches from a Gaussian decay to an exponential decay (Markovian limit). To extract the coherence lifetimes τ, we fit $\mathrm{Re}[\rho_{+-}(t)]$ to the product of a cosine function and a single exponential decay function

$$\mathrm{Re}[\rho_{+-}(t)] = \frac{1}{2}\cos(\Omega_R \cdot t) \cdot e^{-t/T_2} \tag{20}$$

where the coherence oscillates with a frequency of the Rabi splitting $\Omega_R = 2\sqrt{N}g_c$ (for an isolated two-level system), the coherence decay follows an exponential behavior with the characteristic time T_2 (due to coupling to phonons), and the coherence beatings last until ∼150 fs. eq 20 fits the HEOM data exceptionally well, which are plotted as colored cross markers in each panel, and give the decoherence time T_2 as 61.2 fs (panel a), 100.9 fs (panel b), and 146.5 fs (panel c). For comparison, the coherence lifetime for $\lim_{g_c \to 0^+} \mathrm{Re}[\rho_{+-}(t)]$ is
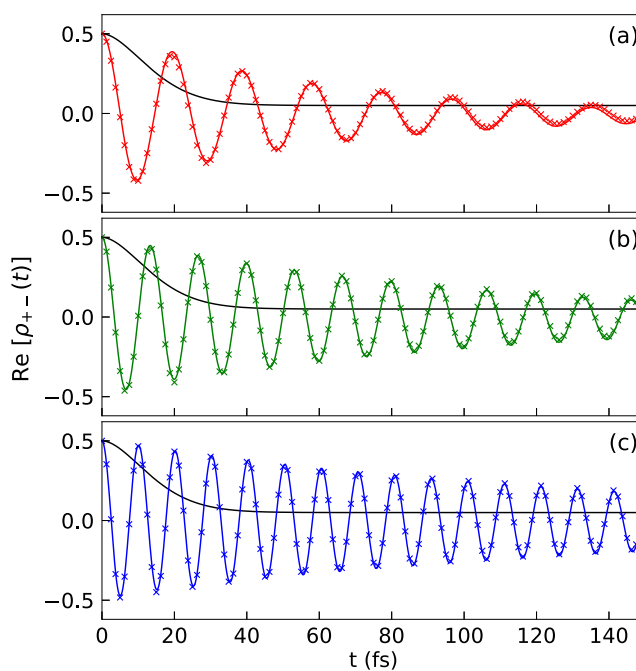

Figure 2. Real part of $\rho_{+-}(t)$ in a lossless cavity. The number of molecules is fixed to be $N = 10$. The collective coupling strengths between the matter state and the cavity mode are (a) $\sqrt{N}g_c = 100$ meV (red), (b) $\sqrt{N}g_c = 150$ meV (green), (c) $\sqrt{N}g_c = 200$ meV (blue). For comparison, $\lim_{g_c \to 0^+} \mathrm{Re}[\rho_{-}(t)]$ is depicted with black solid lines. The real components of $[\hat{\rho}_S]_{+-}(t)$ are fitted to the product of a cosine and a single exponential decay (crossed markers).

$T_2 = 15.7$ fs when fitted to a Gaussian decay profile, which is the typical electronic coherence time under room temperature. Coupling to a cavity can significantly prolong T_2 to ∼60 fs with a realistic collective coupling parameter[54,55] $\sqrt{N}g_c = 100$ meV. In the 2DES experiments of molecular polariton,[36] the largest Rabi splitting achieved was $\Omega_R = 380$ meV (or $\sqrt{N}g_c \approx 190$ meV). The Rabi splitting in the range of $\Omega_R = 420$ meV (or $\sqrt{N}g_c \approx 210$ meV) has been reported when coupling the squaraine dye molecules coupled to the cavity.[36,56] Results in Figure 2 suggest that under the collective coupling of a few molecules with the cavity when N is fixed and increasing g_c, the coherence $\rho_{+-}(t)$ will be increased. This is also the case when $N = 1$, and with an increasing g_c one can significantly prolong the coherence $\rho_{+-}(t)$, as shown in Figure S3 in the Supporting Information. We note that the decoherence mechanism when $N = 1$ is fundamentally different than when $N > 1$ because the former case does not contain any dark state.

Figure 3 presents the decoherence dynamics with a fixed light−matter coupling strength $g_c = 44.7$ meV and only increases the number of molecules N. As such, the coupling strength between the cavity and a single molecule is fixed, but the collective coupling strength $\sqrt{N}g_c$ is increased, due to more molecules being collectively coupled to the cavity mode. The number of molecules is varied from $N = 5$ (panel a) to $N = 10$ (panel b) and $N = 20$ (panel c), such that the collective coupling strength is (a) $\sqrt{N}g_c = 100$ meV, (b) $\sqrt{N}g_c = 141.4$ meV and (c) $\sqrt{N}g_c = 200$ meV, identical or similar to those presented in Figure 2. Most of the experimental setups in
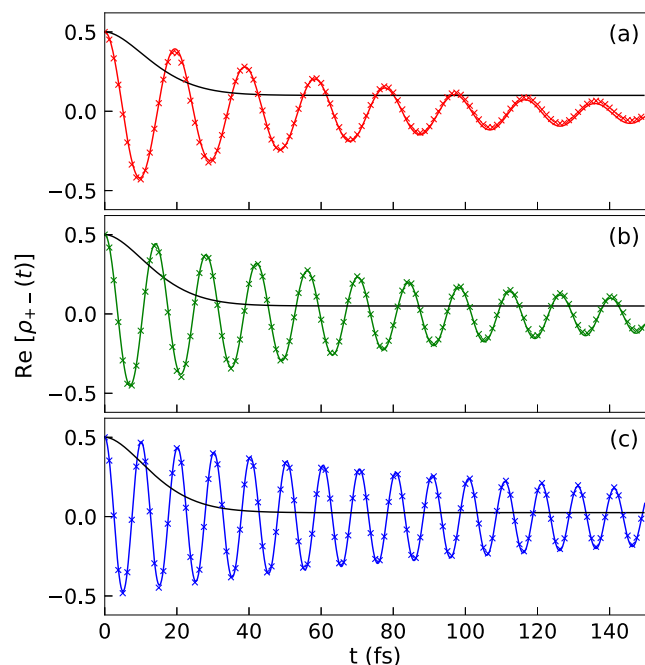
Figure 3. $\mathrm{Re}[\rho_{+-}(t)]$ for a fixed g_c while varying N. The single molecule coupling strength is g_c = 44.7 meV. The number of molecules used is (a) N = 5 (red), (b) N = 10 (green), and (c) N = 20 (blue). The results are obtained from the HEOM simulations (solid curve) as well as the fitting with eq 20 (crossed markers).

Figure 4. Population of UP ($|+\rangle$ state), LP ($|-\rangle$ state) and dark states (DS) that sums all $\{|D_k\rangle\}$ states population for a fixed single molecule coupling strength g_c = 44.7 meV, with the number of molecules (a) N = 1 (no dark states), (b) N = 5, and (c) N = 20.

molecular polaritons are similar to this case, where the individual coupling to each molecule is fixed and the collective Rabi splitting $\Omega_R = 2\sqrt{N}g_c$ is increased due to an increase in N. The decoherence dynamics can also be fitted very well using eq 20, with extracted coherence lifetime as (a) T_2 = 67.2 fs, (b) T_2 = 94.2 fs, and (c) T_2 = 141.4 fs. For comparison, we also extract the coherence lifetime for $\lim_{g_c \to 0^+} \mathrm{Re}[\rho_{+-}(t)]$ (with a Gaussian fitting), resulting in (a) T_2 = 16.7 fs, (b) T_2 = 15.7 fs, and (c) T_2 = 15.2 fs. Thus, under the collective coupling regime and with an increasing N, $\mathrm{Re}[\rho_{+-}(t)]$ decay at a slower rate and the coherence lifetimes for the coupled states are about 4 to 9.3 times greater than the coherence lifetime for the uncoupled system. Further, comparing to Figure 2, one observes that the decoherence dynamics are nearly identical with each other, as long as the collective coupling strength $\sqrt{N}g_c$ is the same. To be clear, the Hamiltonian in Figure 2 is different compared to Figure 3. The former is fixing N and varying g_c, and the latter one is fixing g_c and varying N. Nevertheless, it seems that the decoherence dynamics is only sensitive to $\sqrt{N}g_c$, agreeing with the empirical rule in the early numerical simulations with Lindblad dynamics.[57]

To understand the decoherence mechanism under the collective coupling regime and make sense of the exact numerical results presented in Figures 2-3, we focus on the population dynamics presented in Figure 4. One can see that there is a significant population transfer from the $|+\rangle$ state to the dark state manifold $\{|D_k\rangle\}$, such that the decoherence mechanism is *not* pure-dephasing (which does not have any population transfer). This also makes the decoherence mechanism for the collective coupling case ($N \neq 1$) fundamentally different from the single molecule case (N = 1), because the latter does not have any dark state. For the
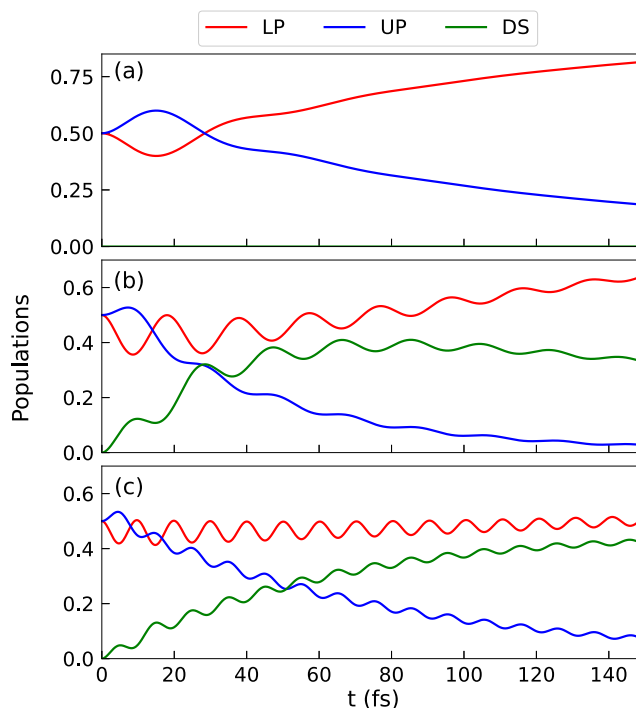
collective coupling regime, the main contribution for the $\rho_{+-}(t)$ decoherence, as shown in Figure 4, is the population transfer from $|+\rangle$ state to the dark states manifold $\{|D_k\rangle\}$. In Figure 4c (where N = 20), we can see that $\rho_{++}(t)$ population gradually decay from 1/2 and the dark state population $\rho_{DD}(t)$ gradually increase, whereas the $\rho_{--}(t)$ population oscillates around a certain value but do not increase significantly. This means that the main mechanism of $\rho_{+-}(t) = c_+^*(t) \cdot c_-(t)$ decay is due to the decrease of $c_+^*(t)$ (because of $\rho_{++}(t) = c_+^*(t) \cdot c_+(t)$ decay), and $c_-(t)$ does not have a significant change (due to the fact that $\rho_{--}(t) = c_-^*(t) \cdot c_-(t)$ does not significantly increase).

To obtain an insight into the decoherence mechanism, we derive an analytic expression of the coherence time. We begin by transforming the total Hamiltonian in eq 1 into the polariton state and Dark state basis $\{|\pm\rangle, D_k\}$. Because these states are the eigenstates of $\hat{H}_s$ (eq 10), they will make $\hat{H}_s$ purely diagonal. Transitions among these states are induced by the phonon couplings, specifically from $\hat{H}_{sb}$ (eq 4b). The full Hamiltonian expression in this polariton basis is provided in Sec. I of the Supporting Information. Here, we focus on $\hat{H}_{sb}$ (eq 4b) in the polaritonic basis $\hat{H}_{sb} = \hat{\mathcal{H}}_\pm + \hat{\mathcal{H}}_{\{\pm,D\}} + \hat{\mathcal{H}}_D$, where $\hat{\mathcal{H}}_\pm$ provides the phonon-mediated transitions between $|+\rangle$ and $|-\rangle$ states, $\hat{\mathcal{H}}_{\{\pm,D\}}$ provides the phonon-mediated transitions between the $|\pm\rangle$ states to the dark state manifolds $\{|D_k\rangle\}$, and $\hat{\mathcal{H}}_D$ provides the phonon-mediated transitions among dark states. In particular, under the resonance condition Δ = 0 (eq 13), the mixing angle is $\Theta_N = \pi/4$, $\hat{\mathcal{H}}_\pm$ and $\hat{\mathcal{H}}_{\{\pm,D\}}$ are expressed as follows

$$\hat{\mathcal{H}}_{\pm} = \frac{1}{2}(|+\rangle\langle+| + |-\rangle\langle-|) \otimes \sum_{\alpha} \frac{c_{\alpha}}{\sqrt{N}}(\hat{b}_{\alpha,0} + \hat{b}^{\dagger}_{\alpha,0})$$
$$- \frac{1}{2}(|+\rangle\langle-| + |-\rangle\langle+|) \otimes \sum_{\alpha} \frac{c_{\alpha}}{\sqrt{N}}(\hat{b}_{\alpha,0} + \hat{b}^{\dagger}_{\alpha,0})$$
$$(21a)$$

$$\hat{\mathcal{H}}_{\{\pm,D\}} = \sum_{k=1}^{N-1} |D_k, 0\rangle\langle+| \otimes \sum_{\alpha} \frac{c_{\alpha}}{\sqrt{2N}}(\hat{b}_{\alpha,k} + \hat{b}^{\dagger}_{\alpha,-k})$$
$$- \sum_{k=1}^{N-1} |D_k, 0\rangle\langle-| \otimes \sum_{\alpha} \frac{c_{\alpha}}{\sqrt{2N}}(\hat{b}_{\alpha,-k} + \hat{b}^{\dagger}_{\alpha,k}) + \text{h. c.}$$
$$(21b)$$

where h.c. stands for the Hermitian Conjugate, and the general expression with an arbitrary Θ_N is provided in Sec. I of the Supporting Information. In the above expressions, $\hat{b}_{\alpha,k} = \frac{1}{\sqrt{N}}\sum_{n=0}^{N-1}\exp\left(-2\pi i\frac{nk}{N}\right)\hat{b}_{\alpha,n}$ and $\hat{b}^{\dagger}_{\alpha,k} = \frac{1}{\sqrt{N}}\sum_{n=0}^{N-1}\exp\left(-2\pi i\frac{nk}{N}\right)\hat{b}^{\dagger}_{\alpha,n}$ are the creation and annihilation operators of the α_{th} bath phonon mode for the k_{th} eigenstates of $\hat{H}_s$. The special symmetrical phonon modes are $\hat{b}_{\alpha,0} = \frac{1}{\sqrt{N}}\sum_{n=1}^{N}\hat{b}_{\alpha,n}$ and $\hat{b}^{\dagger}_{\alpha,0} = \frac{1}{\sqrt{N}}\sum_{n=1}^{N}\hat{b}^{\dagger}_{\alpha,n}$, which only couple to the $|\pm\rangle$ states (see eq 21a).

From eq 21a, one can see that both $|+\rangle$ state and $|-\rangle$ state are coupled to the phonon modes $\hat{R}_{\alpha,0} = (\hat{b}_{\alpha,0} + \hat{b}^{\dagger}_{\alpha,0})/\sqrt{2\omega_{\alpha}}$, for both the diagonal term (Holstein coupling) and off-diagonal term (Peierls coupling), with a rescaled coupling strength $c_{\alpha}/\sqrt{N}$. Note that the displacement between the $|G, 0\rangle$ and the $|\pm\rangle$ states is given by[40] $\mathcal{R}_{\alpha,0} = R_{\alpha,0}/2\sqrt{N}$, where $R_{\alpha,0} = \sqrt{2c_{\alpha}^2/\omega_{\alpha}^3}$ is the displacement between the $|E_n, 0\rangle$ and $|G, 0\rangle$ states. Thus, the effective reorganization energy $\lambda_N = \frac{1}{2}\sum_{\alpha}\omega_{\alpha}^2\mathcal{R}_{\alpha,0}^2$ between the $|G, 0\rangle$ state and the $|\pm\rangle$ states is

$$\lambda_N = \frac{\lambda}{4N} \qquad (22)$$

This means that under the $N \to \infty$ limit (in experiments of organic polaritons, one estimates $N \sim 10^6 - 10^{12}$, and in NPL-cavity polaritons,[42] $N \sim 10^3 - 10^4$), the direct phonon couplings are completely decoupled from the $|\pm\rangle$ states.[40] As such, the optical line shape (such as polariton absorption) that corresponds to $|G, 0\rangle \to |\pm\rangle$ optical transition will become much narrower than systems outside the cavities,[40] and this will also present itself in the diagonal peaks of the 2DES spectra.[36] However, polaron decoupling (eq 22) is not responsible for a longer $\rho_{+-}(t)$ coherence time when increasing $\sqrt{N}g_c$ as we have observed in Figures 2-3. This is because although both $|+\rangle$ and $|-\rangle$ have a relative shift $R_{\alpha,0}$ with respect to $|G, 0\rangle$ (polaron decoupling), there is no absolute shift among $|+\rangle$ and $|-\rangle$ states on the diagonal term as can be seen from the first line of eq 21a. Instead, what could contribute to the pure decoherence is the off-diagonal Peierls term that will be discussed later (see eq 24), although this is *not* the main contribution.

The main contribution of the decoherence of ρ_{+-}, on the other hand, originates from the population transfer from the $|+\rangle$ state to the dark states manifold $\{|D_k\rangle\}$. This population transfer process happens within the same time scale of the

$\rho_{+-}(t)$ decoherence process, as shown in Figure 3c and Figure 4c. This transition is caused by the phonon coupling term $\hat{\mathcal{H}}_{\{\pm,D\}}$ in eq 21b. One can estimate the transition rate constant for the process $|+\rangle \to \{|D_k\rangle\}$ using Fermi's Golden Rule (FGR), which gives

$$k_{+\to D} = \frac{N-1}{N}\cdot J_{\nu}(\sqrt{N}g_c)\cdot[\bar{n}(\sqrt{N}g_c) + 1] \qquad (23)$$

where $J_{\nu}(\omega)$ is the phonon spectral density expressed in eq 5, and $\bar{n}(\omega) = 1/(e^{\beta\hbar\omega} - 1)$ is the Bose–Einstein distribution function of the phonon. Note that the energy gap between $|+\rangle$ and $|D_k\rangle$ is $\omega_+ - \omega_D = \Omega_R/2 = \sqrt{N}g_c$, which appears in $J_{\nu}(\omega)$ and $\bar{n}(\omega)$ of the FGR expression. For an arbitrary detuning case, there will be an additional factor $[1 + \cos(2\Theta_N)]$ in the FGR expression, see eq S21c in the Supporting Information. The scaling $(N-1)/N$ in eq 23 is well-known,[58−60] because there are $N-1$ dark state to transfer to, and the $1/N$ is originated from the rescaled phonon coupling $c_{\alpha}/\sqrt{N}$. Further, $k_{+\to D}$ can already explain the similarity of the decoherence dynamics we observed in Figures 2−3. This is because when N is sufficiently large, $(N - 1/N) \sim 1$, and the relaxation rate for the $|+\rangle \to \{|D_k\rangle\}$ process is completely dictated by $\sqrt{N}g_c$ as this is the only quantity shown in $k_{+\to D}$ (eq 23). As such, even though the Hamiltonians used in Figure 2 and Figure 3 are different (especially for the number of the dark states), the reduced system dynamics in the $\{|\pm\rangle, |D_k\rangle\}$ are isomorphic to each other as long as $\sqrt{N}g_c$ is identical and N is sufficiently large, and if the dynamics is largely dictated by $|+\rangle \to \{|D_k\rangle\}$ transition.

The off-diagonal Peierls coupling in eq 21a, on the other hand, is the main cause of *pure decoherence* when one does not consider population transfer between $|+\rangle$ and $|-\rangle$ or population transfer to the dark states. This term is also the main cause of decoherence when $N = 1$ (as there is no dark state in this case). One can also estimate the rate constant for the process of $|+\rangle \to |-\rangle$ using FGR, and this rate constant is

$$k_{+\to-} = \frac{1}{2N}\cdot J_{\nu}(2\sqrt{N}g_c)\cdot[\bar{n}(2\sqrt{N}g_c) + 1] \qquad (24)$$

Note that the energy gap is $\omega_+ - \omega_- = \Omega_R = 2\sqrt{N}g_c$, which shows up in the $J_{\nu}(\omega)$ and $\bar{n}(\omega)$ expressions of the FGR. Further, compared to $k_{+\to D}$, the overall scaling is just $1/N$.

With the above two population transfer rate constants (eq 23 and eq 24), we approximate the total coherence lifetime T_2 as

$$\frac{1}{T_2} = \frac{1}{2T_1} + \frac{1}{T_2^*} = \frac{1}{2}k_{+\to D} + \frac{1}{2}k_{+\to-} \qquad (25)$$

where $1/T_1 = k_{+\to D}$, and we assume that for the pure decoherence rate it is half of the population transfer rate between $|+\rangle$ and $|-\rangle$ states (which is indeed valid under the Markovian approximation and this can be seen from the Lindblad master equations[59,60]). Under the large N limit (or collective strong coupling limit), $\sqrt{N}g_c \gg \gamma$, the spectral density $J_{\nu}(\sqrt{N}g_c) \sim 1/\sqrt{N}g_c$ (c.f. eq 5), and we find the following fundamental scalings

$$T_1 \sim N^{3/2}g_c/(N-1), \qquad T_2^* \sim N^{3/2}g_c \qquad (26)$$

Note that in the above scaling law, we explicitly assumed that $\beta\sqrt{N}g_c \gg 1$, such that $1+\bar{n} \approx 1$. This is indeed the case for exciton-polaritons under room temperature conditions $k_BT \approx 26$ meV and $\sqrt{N}g_c > 50$ meV. For lower temperature or vibrational strong coupling cases (where usually $\sqrt{N}g_c < 10$ meV) one also needs to explicitly consider the scaling coming from $\bar{n}(\sqrt{N}g_c)$ and $\bar{n}(2\sqrt{N}g_c)$. Further, the scaling in eq 26 will depend upon the detailed form of the spectral density $J_\nu(\omega)$, but one is guaranteed to figure out this scaling once the detailed form of $J_\nu(\omega)$ is known. Thus, for large N, $T_2^* \gg 2T_1$, and we see that the contribution of the coherence decay rate between $|+\rangle$ and $|-\rangle$ state to T_2 is negligible; the decoherence time for the collective coupling case is

$$\frac{1}{T_2} \approx \frac{1}{2T_1} \sim \frac{N-1}{N^{3/2}g_c} \tag{27}$$

which is the *first key result* of this Letter. On the other hand, when $N = 1$ (single molecule case), $T_1 \sim \infty$ (c.f. eq 26) because there is no dark state at all, the decoherence mechanism is dominated by population transfer between $|+\rangle$ and $|-\rangle$, as shown in Figure 4a. As such, for the single molecule case

$$\frac{1}{T_2} \approx \frac{1}{T_2^*} = \frac{1}{2}\frac{\lambda\gamma g_c}{\gamma^2 + 4g_c^2}[\bar{n}(2g_c) + 1] \sim \frac{1}{g_c} \tag{28}$$

which reflects a simple fact that as $\omega_{+-} = \omega_+ - \omega_- = 2g_c$ gets larger, the phonon in J_ν cannot efficiently mediate the transition $|+\rangle \rightarrow |-\rangle$ unless there is a high frequency phonon that matches ω_{+-}. Note that the simple scaling at the end of eq 28 only works when $g_c \gg \gamma$, otherwise $1/T_2^*$ will exhibit a turnover, dictated by the form of $J_\nu(2g_c)$ (c.f. eq 5). Nevertheless, we have observed this from direct theoretical simulations of 2DES spectra of a single molecule strongly coupled to the cavity,[32] and indeed find that the longer coherence time can be achieved by increasing g_c. Further, earlier theoretical work also suggests that one can prolong the ρ_{+-} coherence by increasing g_c from the potential energy surface hybridization perspective.[31] Additional numerical results are provided in Sec. VI of the Supporting Information to characterize the ρ_{+-} decoherence for $N = 1$ with increasing g_c. However, we emphasize that the fundamental mechanism for decoherence in the $N = 1$ case (eq 28) is different compared to the collective coupling case (eq 27).

Figure 5 presents a numerical check of the scaling predicted by eq 27, where we have simulated three cases: (a) fixing the collective coupling $\sqrt{N}g_c = 180$ meV while increasing N (and thus decrease g_c accordingly, (b) fixing $g_c = 44.7$ meV while increasing N, and (c) fixing $N = 10$ while increasing g_c. The results are obtained from HEOM simulations and extracted using eq 20 (red dots), the least-squares fitting using the corresponding scaling (blue curve), as well as from FGR using eq 25 (green).

According to the scaling predicted by FGR, $2T_1$ scales as $N/(N-1)$ when $\sqrt{N}g_c$ is fixed, scales as $N^{3/2}/(N-1)$ when g_c is fixed, and scales as g_c when N is fixed. As one can see, the least-squares fittings match the HEOM data for all three panels in Figure 5 and show that our scaling arguments are correct. Furthermore, we see that the FGR expression overestimates the T_2 value by only 40 fs, likely due to ignoring the other
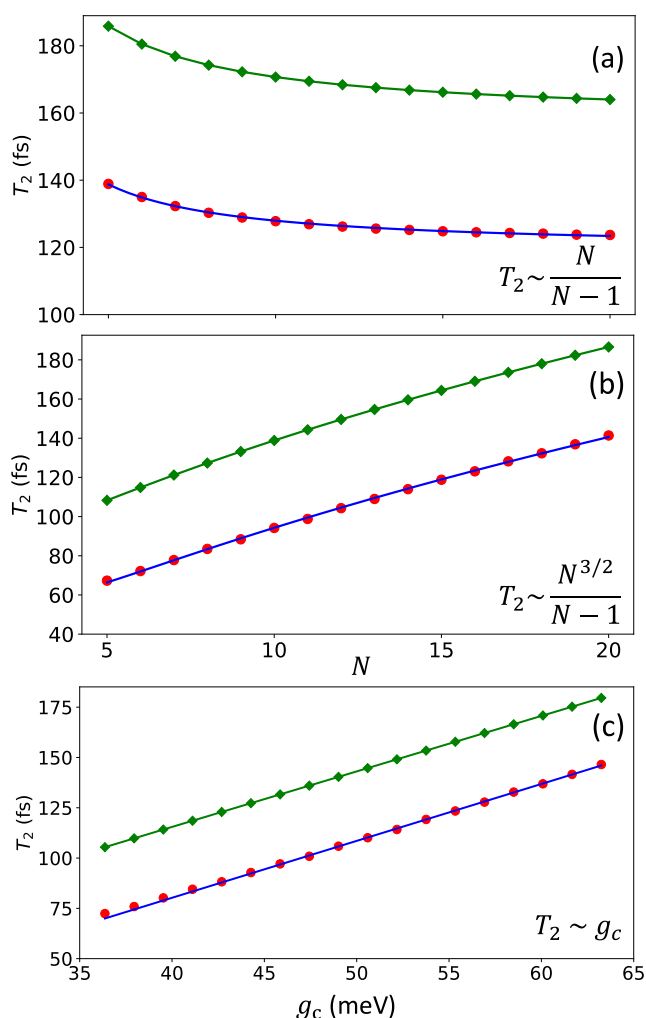

Figure 5. Fundamental scaling relation of the coherence lifetime T_2 with respect to N and g_c for various systems. The results are obtained from HEOM exact simulation (red dots), and compared to the fitting line (blue solid lines) and from FGR estimations (green dot-line). (a) T_2 as a function of N when $\sqrt{N}g_c = 180$ meV is fixed (such that when N increase, g_c decreases accordingly). (b) T_2 as a function of N for fixed $g_c = 44.7$ meV. (c) T_2 as a function of g_c for fixed N.

contribution of decoherence (that further reduces T_2.) Thus, we note that eqs 23 and (24) not only reproduce the scaling of T_2 with respect to the system parameters, but they also provide a reasonable estimate for the actual coherence lifetimes predicted by exact quantum dynamics. We expect these equations to be of use in interpreting experimental results that couple many molecules strongly to a cavity, such as polariton spectral line width.[32,36] Further, we demonstrate the robustness of the prolonged coherence $\rho_{+-}(t)$ when explicitly considering cavity loss. To incorporate the cavity loss effect, we couple the cavity mode with a lossy environmental DOF corresponding to the photonic modes outside the cavity (far field modes).[61,62] This part of the Hamiltonian is expressed as

$$\hat{H}_{\text{loss}} = \sum_\alpha \frac{\hat{P}_\alpha^2}{2} + \frac{1}{2}\tilde{\omega}_\alpha^2\left[\hat{Q}_\alpha + \frac{C_\alpha}{\tilde{\omega}_\alpha^2}(\hat{a}^\dagger + \hat{a})\right]^2$$

where $\tilde{\omega}_\alpha$ is the frequency of the modes, and C_α is the coupling strength between the cavity mode and the photon loss bath.

The photon loss bath is modeled with a Drude-Lorentz spectral density

$$J_{\text{loss}}(\omega) = \frac{\pi}{2} \sum_{\alpha} \frac{C_\alpha^2}{\tilde{\omega}_\alpha} \delta(\omega - \tilde{\omega}_\alpha) = \frac{2\lambda_c \omega \gamma_c}{\omega^2 + \gamma_c^2}$$

Using the expression for the cavity loss rate[61,62] (see derivation in ref 62, Appendix D)

$$\tau_c^{-1} = J_{\text{loss}}(\omega_c)/[\omega_c(1 - e^{-\beta\omega_c})] \tag{29}$$

where $\omega_c = (\omega_x + \lambda) + \Delta$, with Δ as the light−matter detuning, and the cavity quality factor is defined as $Q = \omega_c \tau_c$. Here, we choose the parameters $\lambda_c = 5.15$ meV and $\gamma_c = 800$ meV for the cavity loss bath, corresponding to a cavity loss rate $\tau_c^{-1}=8.83$ meV (c.f. eq 29) or a quality factor of $Q \approx 266$ (when $\omega_c = 2$ eV), which is a typical experimental loss rate in a distributed Bragg reflector (DBR) cavity.[42] This loss spectral density $J_{\text{loss}}(\omega)$ in eq 29 is included in the HEOM exact quantum dynamics simulations. Of course, cavity loss also significantly contributes to the population decay of the $|+\rangle$ state, and one can estimate the decoherence rate as $\frac{1}{T_2} \approx \frac{1}{2}k_{+\to D} + \frac{1}{2}\tau_c^{-1}$, where 1/2 of the character of $|+\rangle$ is the photonic character $|G, 1\rangle$, and the decoherence rate due to cavity loss is 1/2 of the photonic population decay rate τ_c^{-1}.

Figure 6 presents the $\rho_{+-}(t)$ in a lossy cavity for fixed g_c, same as those in Figure 3, except with the inclusion of cavity
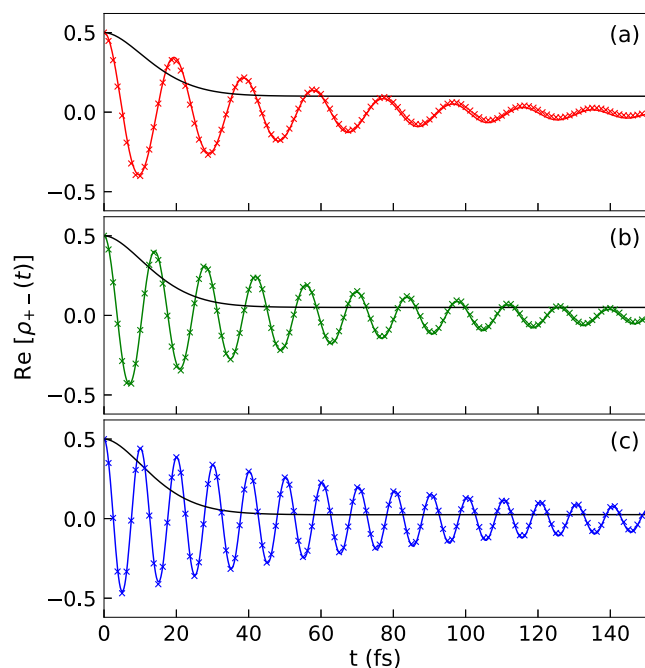

Figure 6. Same parameters as in Figure 3 with (a) $N = 5$ (red), (b) $N = 10$ (green), and (c) $N = 20$ (blue), but with cavity loss rate $\tau_c^{-1} = 8.83$ meV.

loss in the HEOM simulation. The extracted coherence lifetimes (using eq 20) are (a) $T_2 = 46.6$ fs for $\sqrt{N}g_c = 100$ meV, (b) $T_2 = 58.9$ fs for $\sqrt{N}g_c = 141.4$ meV, and c) $T_2 = 77.6$ fs for $\sqrt{N}g_c = 200$ meV. One can see that Re$[\rho_{+-}(t)]$ indeed decays faster in a lossy cavity compared to a perfect cavity, but coherence between $|+\rangle$ and $|-\rangle$ still lasts much longer compared to the typical value of electronic decoherence rate.

For example, when $\sqrt{N}g_c = 200$ meV (Figure 6c) the decoherence time is 77.6 fs when having a cavity loss rate of $\tau_c^{-1}=8.83$ meV, which is about 3 times longer than the outside cavity case. Thus, the presence of strong collective light−matter coupling still enhances the quantum coherence of the bright polaritonic states even in the presence of cavity loss.

Figure 7 shows the coherence lifetimes T_2 for a finite light−matter detuning $\Delta = \omega_c - (\omega_x + \lambda)$. We consider the
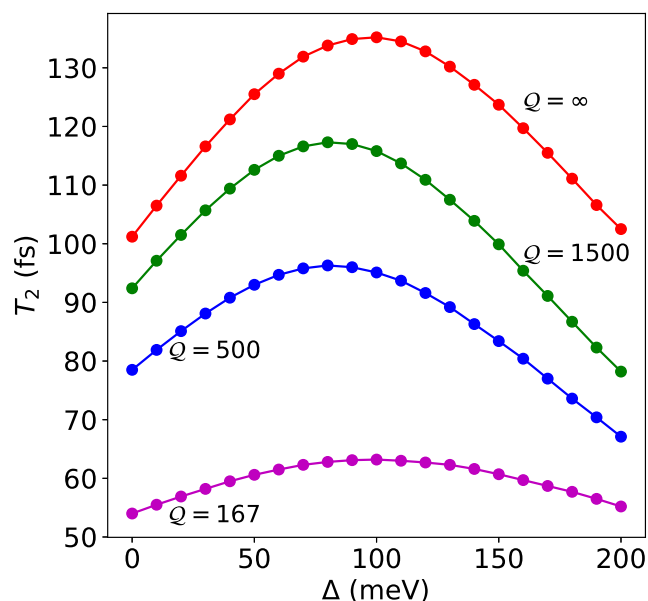

Figure 7. T_2 for fixed collective coupling strength $\sqrt{N}g_c = 150$ meV, while varying light−matter detuning Δ. The coherence lifetimes for lossy cavities with quality factors of $Q = 167$ (magenta), $Q = 500$ (blue) and $Q = 1500$ (green) are plotted with the lifetimes in a lossless cavity (red).

coherences in both lossless and lossy cavities, and for lossy cavities, we have quality factors from $Q = 167$ to $Q = 1500$ that are representative of experimentally realizable optical cavities.[19,42] For positive Δ, T_2 increases with increasing Δ until it reaches a turnover point where T_2 decreases with further increases in Δ. From our FGR analysis, this turnover is caused by the competition between the population transfer from $|+\rangle \to \{|D_k\rangle\}$ given by the rate $k_{+\to D}$, and the population transfer from $|-\rangle \to \{|D_k\rangle\}$ given by the rate $k_{-\to D}$. We also include the photonic loss to the $|G, 1\rangle$ state from the $|\pm\rangle$ states. Combining all contributions to the decoherence rate, we have the *second key result* of this Letter

$$\frac{1}{T_2} \approx \frac{2(N - 1)}{N}\left[-\frac{\partial \Delta E_-}{\partial \Delta} \cdot J_\nu(\Delta E_+) \cdot (\overline{n}(\Delta E_+) + 1)\right.$$
$$\left. + \frac{\partial \Delta E_+}{\partial \Delta} \cdot J_\nu(\Delta E_-) \cdot \overline{n}(\Delta E_-)\right] + \frac{1}{2}\tau_c^{-1} \tag{30}$$

where the energy gap between $|+\rangle$ and dark state as well as between dark state to $|-\rangle$ is

$$\Delta E_\pm = \pm\frac{\Delta}{2} + \frac{1}{2}\sqrt{\Delta^2 + 4Ng_c^2} \tag{31}$$

and

$$\pm \frac{\partial \Delta E_{\pm}}{\partial \Delta} = \frac{1}{2}\left(1 \pm \frac{\Delta}{\sqrt{\Delta^2 + 4Ng_c^2}}\right)$$

(32)

are the Hopfield coefficients.[9,42] In eq 30, we have explicitly ignored the $1/T_2^*$ contribution (c.f. eq 23 and eq 25). With a larger light−matter detuning Δ, the first term in eq 31 decreases due to a reduced $J_\nu(\Delta E_+)$ originated from a larger energy gap between $|+\rangle$ state and the dark states manifold. On the other hand, the second term in eq 31 increases because of increased $J_\nu(\Delta E_-)$ with a smaller energy gap between $|-\rangle$ state and the dark states manifold. As such, there will be a *turnover* of $1/T_2$ as one increases the light−matter detuning $\Delta = \omega_c - (\omega_x + \lambda)$ from zero value to positive values. Also note that in eq 30, we have explicitly considered the contribution from both UP and LP, as opposed to the zero detuning cases where we only considered the contributions from UP to dark states. This is because, for $\Delta = 0$, the population transfer from LP to dark states is energetically uphill and less favorable (negligible in the current model system, see Figure 4). When $\Delta \neq 0$, the population transitions from both UP and LP to the dark states need to be considered, especially for the positive detuning case when the LP energy is close to the dark exciton energies.

The impact of cavity loss, which affects both $|\pm\rangle$ states, is to cause additional decoherence from population transfer to the $|G, 1\rangle$ state. Figure 7 verify such a turnover of T_2 as a function of the detuning obtained from HEOM simulations, at various cavity quality factors from $Q = 167$ to $Q = 1500$. Further analysis of the turnover using the formalism of eq 30 is provided in Sec. VIII of the Supporting Information. Note that in principle, τ_c is also a function of the detuning (or cavity frequency ω_c) if the loss dynamics is not Markovian (c.f. eq 29).

In this Letter, we theoretically demonstrate that the coherence lifetime between the upper and lower polariton states in the collective coupling regime increases with an increasing collective Rabi splitting $2\sqrt{N}g_c$. This is confirmed by computing $\rho_{+-}(t)$ using exact quantum dynamics simulation through the HEOM approach, as well as through analytic rate theory using Fermi's Golden Rule. We found that the main mechanism for decoherence under this collective coupling regime at resonance condition largely comes from population transfer from the upper polariton state to the dark states manifold, a departure from the pure dephasing limit that does not involve any population transfer. Using analytic theory based on FGR expression, we showed that polariton decoherence can be mitigated by reducing exciton−phonon couplings. An enlarged energy gap between the polariton states and the dark states further reduces the population relaxation rate from $|+\rangle$ to the dark state manifold, as well as the decoherence rate. Further, we showed that this enhancement in coherence is robust even in the presence of cavity loss, with a range of quality factors that can be achieved using the state-of-the-art FP cavities.[42,46] By investigating the coherence enhancements with varying light−matter detunings, we further demonstrated the importance of the dark states in mediating the coherences between the polaritonic states and theoretically predicted and explained the turnover in T_2 for positive Δ as a consequence of competition between transitions from $|+\rangle \rightarrow \{|D_k\rangle\}$ and $|-\rangle \rightarrow \{|D_k\rangle\}$.

We point out again that in most existing experiments, N is much larger than what we can directly simulate through exact quantum dynamics simulation. In experiments of organic polaritons, one estimates $N \sim 10^6 - 10^{12}$, and in NPL-cavity polaritons,[42] $N \sim 10^3 - 10^4$. Nevertheless, we do expect that the decoherence mechanism discovered in this work is the same as N approaches to a very large number, in the sense that (1) the main mechanism for the decay of $\rho_{+-}(t)$ remains the population transfer from $|+\rangle$ to $\{|D_k\rangle\}$, and (2) this population transfer rate is only sensitive to a collective quantity $\sqrt{N}g_c$ that enters into the FGR expression.[63] As such, we expect for the very large N limit that one uses the $N/(N-1) \approx 1$ approximation for all expressions in this work. Of course, direct numerical simulations will be ideal to test these further, and is subject to future work with efficient algorithms[64] that take advantage of the sparsity and symmetry of the HTC Hamiltonian.

Finally, the results in this Letter use parameters that are representative of those found in recent polariton experiments with CdSe NPL coupled to DBR FP cavities.[42,46] We thus expect that these theoretical predictions can be directly verified experimentally and will provide crucial insights into understanding polariton 2D spectroscopy data.[36]

■ ASSOCIATED CONTENT

ⓢ Supporting Information

The Supporting Information is available free of charge at https://pubs.acs.org/doi/10.1021/acs.jpclett.4c03049.

> Details of the HTC system in the polaritonic basis; FGR rates for polariton transitions; details of HEOM simulations; purity results for a fixed number of molecules; coherence data for a fixed number of molecules in a lossy cavity; coherence data for single molecule case ($N = 1$); discussion of Gaussian to Markovian transition in the collective coupling regime; FGR analysis of the decoherence turnover with increasing positive detunings (PDF)

> Transparent Peer Review report available (PDF)

■ AUTHOR INFORMATION

Corresponding Author

Pengfei Huo − *Department of Chemistry, The Institute of Optics, Hajim School of Engineering, and Center for Coherence and Quantum Optics, University of Rochester, Rochester, New York 14627, United States;* ⓞ orcid.org/0000-0002-8639-9299; Email: pengfei.huo@rochester.edu

Authors

Benjamin X. K. Chng − *Department of Physics and Astronomy, University of Rochester, Rochester, New York 14627, United States;* ⓞ orcid.org/0009-0001-1368-8719

Wenxiang Ying − *Department of Chemistry, University of Rochester, Rochester, New York 14627, United States;* ⓞ orcid.org/0000-0003-3188-020X

Yifan Lai − *Department of Chemistry, University of Rochester, Rochester, New York 14627, United States*

A. Nickolas Vamivakas − *Department of Physics and Astronomy, University of Rochester, Rochester, New York 14627, United States; The Institute of Optics, Hajim School of Engineering and Center for Coherence and Quantum Optics, University of Rochester, Rochester, New York 14627, United States;* ⓞ orcid.org/0000-0003-4253-1611

Steven T. Cundiff − *Department of Physics, University of Michigan, Ann Arbor, Michigan 48109, United States;* orcid.org/0000-0002-7119-5197

Todd D. Krauss − *Department of Chemistry, The Institute of Optics, Hajim School of Engineering, and Center for Coherence and Quantum Optics, University of Rochester, Rochester, New York 14627, United States;* orcid.org/0000-0002-4860-874X

■ REFERENCES

(1) Kavokin, A.; Malpuech, G. *Cavity polaritons*; Elsevier, 2003.

(2) Weisbuch, C.; Nishioka, M.; Ishikawa, A.; Arakawa, Y. Observation of the coupled exciton-photon mode splitting in a semiconductor quantum microcavity. *Physical review letters* **1992**, *69*, 3314.

(3) Pekar, S. The theory of electromagnetic waves in a crystal in which excitons are produced. *Sov. Phys. JETP* **1958**, *6*, 785.

(4) Schneider, C.; Rahimi-Iman, A.; Kim, N. Y.; Fischer, J.; Savenko, I. G.; Amthor, M.; Lermer, M.; Wolf, A.; Worschech, L.; Kulakovskii, V. D.; et al. An electrically pumped polariton laser. *Nature* **2013**, *497*, 348−352.

(5) Christopoulos, S.; Von Högersthal, G. B. H.; Grundy, A.; Lagoudakis, P.; Kavokin, A.; Baumberg, J.; Christmann, G.; Butté, R.; Feltin, E.; Carlin, J.-F.; et al. Room-temperature polariton lasing in semiconductor microcavities. *Physical review letters* **2007**, *98*, 126405.

(6) Kéna-Cohen, S.; Forrest, S. Room-temperature polariton lasing in an organic single-crystal microcavity. *Nat. Photonics* **2010**, *4*, 371−375.

(7) Freire-Fernández, F.; Sinai, N. G.; Tan, M. J. H.; Park, S. M.; Koessler, E. R.; Krauss, T. D.; Huo, P.; Odom, T. W. Room-Temperature Polariton Lasing from CdSe core-only Nanoplatelets. *ACS Nano* **2024**, *18*, 15177−15184.

(8) Kasprzak, J.; Richard, M.; Kundermann, S.; Baas, A.; Jeambrun, P.; Keeling, J. M. J.; Marchetti, F.; Szymańska, M.; André, R.; Staehli, J.; et al. Bose−Einstein condensation of exciton polaritons. *Nature* **2006**, *443*, 409−414.

(9) Deng, H.; Haug, H.; Yamamoto, Y. Exciton-polariton bose-einstein condensation. *Reviews of modern physics* **2010**, *82*, 1489.

(10) Keeling, J.; Kéna-Cohen, S. Bose−Einstein condensation of exciton-polaritons in organic microcavities. *Annu. Rev. Phys. Chem.* **2020**, *71*, 435−459.

(11) Ghosh, S.; Liew, T. C. Quantum computing with exciton-polariton condensates. *npj Quantum Information* **2020**, *6*, 16.

(12) Kavokin, A.; Liew, T. C.; Schneider, C.; Lagoudakis, P. G.; Klembt, S.; Hoefling, S. Polariton condensates for classical and quantum computing. *Nature Reviews Physics* **2022**, *4*, 435−451.

(13) Ballarini, D.; De Giorgi, M.; Cancellieri, E.; Houdré, R.; Giacobino, E.; Cingolani, R.; Bramati, A.; Gigli, G.; Sanvitto, D. All-optical polariton transistor. *Nat. Commun.* **2013**, *4*, 1778.

(14) Zasedatelev, A. V.; Baranikov, A. V.; Urbonas, D.; Scafirimuto, F.; Scherf, U.; Stöferle, T.; Mahrt, R. F.; Lagoudakis, P. G. A room-temperature organic polariton transistor. *Nat. Photonics* **2019**, *13*, 378−383.

(15) Liew, T.; Kavokin, A.; Ostatnickỳ, T.; Kaliteevski, M.; Shelykh, I.; Abram, R. Exciton-polariton integrated circuits. *Phys. Rev. B* **2010**, *82*, 033302.

(16) Balasubrahmaniyam, M.; Simkhovich, A.; Golombek, A.; Sandik, G.; Ankonina, G.; Schwartz, T. From enhanced diffusion to ultrafast ballistic motion of hybrid light−matter excitations. *Nat. Mater.* **2023**, *22*, 338.

(17) Liu, B.; Huang, X.; Hou, S.; Fan, D.; Forrest, S. R. Photocurrent generation following long-range propagation of organic exciton−polaritons. *Optica* **2022**, *9*, 1029−1036.

(18) Xu, D.; Mandal, A.; Baxter, J. M.; Cheng, S.-W.; Lee, I.; Su, H.; Liu, S.; Reichman, D. R.; Delor, M. Ultrafast imaging of polariton propagation and interactions. *Nat. Commun.* **2023**, *14*, 3881.

(19) Pandya, R.; Ashoka, A.; Georgiou, K.; Sung, J.; Jayaprakash, R.; Renken, S.; Gai, L.; Shen, Z.; Rao, A.; Musser, A. J. Tuning the Coherent Propagation of Organic Exciton-Polaritons through Dark State Delocalization. *Advanced Science* **2022**, *9*, 2105569.

(20) Schwartz, T.; Hutchison, J. A.; Genet, C.; Ebbesen, T. W. Reversible switching of ultrastrong light-molecule coupling. *Physical review letters* **2011**, *106*, 196405.

(21) Coles, D. M.; Somaschi, N.; Michetti, P.; Clark, C.; Lagoudakis, P. G.; Savvidis, P. G.; Lidzey, D. G. Polariton-mediated energy transfer between organic dyes in a strongly coupled optical microcavity. *Nature materials* **2014**, *13*, 712−719.

(22) Coles, D. M.; Yang, Y.; Wang, Y.; Grant, R. T.; Taylor, R. A.; Saikin, S. K.; Aspuru-Guzik, A.; Lidzey, D. G.; Tang, J. K.-H.; Smith, J. M. Strong coupling between chlorosomes of photosynthetic bacteria and a confined optical cavity mode. *Nat. Commun.* **2014**, *5*, 5561.

(23) Schwartz, T.; Hutchison, J. A.; Léonard, J.; Genet, C.; Haacke, S.; Ebbesen, T. W. Polariton dynamics under strong light−molecule coupling. *ChemPhysChem* **2013**, *14*, 125−131.

(24) Feist, J.; Galego, J.; Garcia-Vidal, F. J. Polaritonic chemistry with organic molecules. *ACS Photonics* **2018**, *5*, 205−216.

(25) Kowalewski, M.; Mukamel, S. Manipulating molecules with quantum light. *Proc. Natl. Acad. Sci. U. S. A.* **2017**, *114*, 3278−3280.

(26) Mandal, A.; Huo, P. Investigating new reactivities enabled by polariton photochemistry. *journal of physical chemistry letters* **2019**, *10*, 5519−5529.

(27) Wang, L.; Allodi, M. A.; Engel, G. S. Quantum coherences reveal excited-state dynamics in biophysical systems. *Nature Reviews Chemistry* **2019**, *3*, 477−490.

(28) Breuer, H.-P.; Petruccione, F.; et al. *The theory of open quantum systems*; Oxford University Press on Demand, 2002.

(29) Weiss, U. *Quantum dissipative systems*; World Scientific, 2012.

(30) Hwang, H.; Rossky, P. J. An analysis of electronic dephasing in the spin-boson model. *J. Chem. Phys.* **2004**, *120*, 11380−11385.

(31) Hu, W.; Gustin, I.; Krauss, T. D.; Franco, I. Tuning and Enhancing Quantum Coherence Time Scales in Molecules via Light-Matter Hybridization. *J. Phys. Chem. Lett.* **2022**, *13*, 11503−11511.

(32) Mondal, M. E.; Koessler, E. R.; Provazza, J.; Vamivakas, A. N.; Cundiff, S. T.; Krauss, T. D.; Huo, P. Quantum dynamics simulations of the 2D spectroscopy for exciton polaritons. *J. Chem. Phys.* **2023**, *159*, 094102.

(33) Herrera, F.; Spano, F. C. Cavity-controlled chemistry in molecular ensembles. *Phys. Rev. Lett.* **2016**, *116*, 238301.

(34) Wu, N.; Feist, J.; Garcia-Vidal, F. J. When polarons meet polaritons: Exciton-vibration interactions in organic molecules strongly coupled to confined light fields. *Phys. Rev. B* **2016**, *94*, 195409.

(35) Scholes, G. D. Polaritons and excitons: Hamiltonian design for enhanced coherence. *Proceedings of the Royal Society A* **2020**, *476*, 20200278.

(36) Takahashi, S.; Watanabe, K. Decoupling from a thermal bath via molecular polariton formation. *J. Phys. Chem. Lett.* **2020**, *11*, 1349−1356.

(37) Tanimura, Y.; Kubo, R. Time evolution of a quantum system in contact with a nearly Gaussian-Markoffian noise bath. *J. Phys. Soc. Jpn.* **1989**, *58*, 101−114.

(38) Yan, Y. Theory of open quantum systems with bath of electrons and phonons and spins: Many-dissipaton density matrixes approach. *J. Chem. Phys.* **2014**, *140*, 054105.

(39) Yan, Y.; Jin, J.; Xu, R.-X.; Zheng, X. Dissipation equation of motion approach to open quantum systems. *Frontiers of Physics* **2016**, *11*, 110306.

(40) Herrera, F.; Spano, F. C. Theory of nanoscale organic cavities: The essential role of vibration-photon dressed states. *ACS photonics* **2018**, *5*, 65−79.

(41) Zeb, M. A.; Kirton, P. G.; Keeling, J. Exact states and spectra of vibrationally dressed polaritons. *ACS Photonics* **2018**, *5*, 249−257.

(42) Qiu, L.; Mandal, A.; Morshed, O.; Meidenbauer, M. T.; Girten, W.; Huo, P.; Vamivakas, A. N.; Krauss, T. D. Molecular polaritons generated from strong coupling between CDSE nanoplatelets and a dielectric optical cavity. *J. Phys. Chem. Lett.* **2021**, *12*, 5030−5038.

(43) Mandal, A.; Taylor, M. A.; Weight, B. M.; Koessler, E. R.; Li, X.; Huo, P. Theoretical advances in polariton chemistry and molecular cavity quantum electrodynamics. *Chem. Rev.* **2023**, *123*, 9786−9879.

(44) Caldeira, A. O.; Leggett, A. J. Quantum tunnelling in a dissipative system. *Annals of physics* **1983**, *149*, 374−456.

(45) Nitzan, A. *Chemical dynamics in condensed phases: relaxation, transfer and reactions in condensed molecular systems*; Oxford University Press, 2006.

(46) Morshed, O.; Amin, M.; Cogan, N.; Koessler, E. R.; Collison, R.; Tumiel, T. M.; Girten, W.; Awan, F.; Mathis, L.; Huo, P.; et al. Room-temperature strong coupling between CdSe nanoplatelets and a metal−DBR Fabry−Pérot cavity. *J. Chem. Phys.* **2024**, *161*, 014710.

(47) Mandal, A.; Krauss, T. D.; Huo, P. Polariton-mediated electron transfer via cavity quantum electrodynamics. *J. Phys. Chem. B* **2020**, *124*, 6321−6340.

(48) Tavis, M.; Cummings, F. W. Exact solution for an N-molecule−radiation-field Hamiltonian. *Phys. Rev.* **1968**, *170*, 379.

(49) Groenhof, G.; Climent, C.; Feist, J.; Morozov, D.; Toppari, J. J. Tracking polariton relaxation with multiscale molecular dynamics simulations. *journal of physical chemistry letters* **2019**, *10*, 5476−5483.

(50) Tichauer, R. H.; Feist, J.; Groenhof, G. Multi-scale dynamics simulations of molecular polaritons: The effect of multiple cavity modes on polariton relaxation. *J. Chem. Phys.* **2021**, *154*, 104112.

(51) Sokolovskii, I.; Tichauer, R. H.; Morozov, D.; Feist, J.; Groenhof, G. Multi-scale molecular dynamics simulations of enhanced energy transfer in organic molecules under strong coupling. *Nat. Commun.* **2023**, *14*, 6613.

(52) Berghuis, A. M.; Tichauer, R. H.; de Jong, L. M.; Sokolovskii, I.; Bai, P.; Ramezani, M.; Murai, S.; Groenhof, G.; Gomez Rivas, J. Controlling exciton propagation in organic crystals through strong coupling to plasmonic nanoparticle arrays. *ACS photonics* **2022**, *9*, 2263−2272.

(53) Prezhdo, O. V.; Rossky, P. J. Relationship between quantum decoherence times and solvation dynamics in condensed phase chemical systems. *Physical review letters* **1998**, *81*, 5294.

(54) Avramenko, A. G.; Rury, A. S. Quantum control of ultrafast internal conversion using nanoconfined virtual photons. *J. Phys. Chem. Lett.* **2020**, *11*, 1013−1021.

(55) Avramenko, A. G.; Rury, A. S. Local molecular probes of ultrafast relaxation channels in strongly coupled metalloporphyrin-cavity systems. *J. Chem. Phys.* **2021**, *155*, 064702.

(56) Cheng, C.-Y.; Krainova, N.; Brigeman, A. N.; Khanna, A.; Shedge, S.; Isborn, C.; Yuen-Zhou, J.; Giebink, N. C. Molecular polariton electroabsorption. *Nat. Commun.* **2022**, *13*, 7937.

(57) Neuman, T.; Aizpurua, J. Origin of the asymmetric light emission from molecular exciton−polaritons. *Optica* **2018**, *5*, 1247−1255.

(58) Pérez-Sánchez, J. B.; Koner, A.; Stern, N. P.; Yuen-Zhou, J. Simulating molecular polaritons in the collective regime using few-molecule models. *Proc. Natl. Acad. Sci. U. S. A.* **2023**, *120*, No. e2219223120.

(59) Pino, J.; Feist, J.; Garcia-Vidal, F. J. Quantum theory of collective strong coupling of molecular vibrations with a microcavity mode. *New J. Phys.* **2015**, *17*, 053040.

(60) Martínez-Martínez, L. A.; Yuen-Zhou, J. Comment on 'Quantum theory of collective strong coupling of molecular vibrations with a microcavity mode. *New J. Phys.* **2018**, *20*, 018002.

(61) Lindoy, L. P.; Mandal, A.; Reichman, D. R. Quantum dynamical effects of vibrational strong coupling in chemical reactivity. *Nat. Commun.* **2023**, *14*, 2733.

(62) Ying, W.; Huo, P. Resonance Theory and Quantum Dynamics Simulations of Vibrational Polariton Chemistry. *J. Chem. Phys.* **2023**, *159*, 084104.

(63) Lai, Y.; Ying, W.; Huo, P. Non-Equilibrium Rate Theory for Polariton Relaxation Dynamics. *J. Chem. Phys.* **2024**, *161*, 104109.

(64) Mondal, M. E.; Vamivakas, A. N.; Cundiff, S. T.; Krauss, T. D.; Huo, P. Polariton Spectra under the Collective Coupling Regime. I. Efficient Simulation of Linear Spectra and Quantum Dynamics. *ChemRxiv* **2024**, 1.